Published in final edited form as:
Neuroimage. 2012 April 2; 60(2): 1073–1082. doi:10.1016/j.neuroimage.2012.01.108.

Gradient Echo Plural Contrast Imaging – signal model and derived contrasts: T2*, T1, Phase, SWI, T1f, FST2*and T2*-SWI

Jie Luo[a], **Bharathi D Jagadeesan**[b], **Anne H Cross**[c], and **Dmitriy A Yablonskiy**[b,d]

[a] Department of Chemistry, Washington University in St. Louis, One Brookings Drive, Saint Louis, MO 63130, USA

[b] Department of Radiology, Washington University in St. Louis, One Brookings Drive, Saint Louis, MO 63130, USA

[c] Departments of Neurology, Washington University in St. Louis, One Brookings Drive, Saint Louis, MO 63130, USA

[d] Departments of Physics, Washington University in St. Louis, One Brookings Drive, Saint Louis, MO 63130, USA

Abstract

Gradient Echo Plural Contrast Imaging (GEPCI) is a post processing technique that, based on a widely available multiple gradient echo sequence, allows simultaneous generation of naturally co-registered images with various contrasts: T1 weighted, R2* = 1/T2* maps and frequency (*f*) maps. Herein, we present results demonstrating the capability of GEPCI technique to generate image sets with additional contrast characteristics obtained by combing the information from these three basic contrast maps. Specifically, we report its ability to generate GEPCI-susceptibility weighted images (GEPCI-SWI) with improved SWI contrast that is free of T1 weighting and RF inhomogeneities; GEPCI-SWI-like images with the contrast similar to original SWI; T1f images that offer superior GM/WM matter contrast obtained by combining the GEPCI T1 and frequency map data; Fluid Suppressed T2* (FST2*) images that utilize GEPCI T1 data to suppress CSF signal in T2* maps and provide contrast similar to FLAIR T2 weighted images; and T2*-SWI images that combine SWI contrast with quantitative T2* map and offer advantages of visualizing venous structure with hyperintense T2* lesions (e.g. MS lesions). To analyze GEPCI images we use an improved algorithm for combining data from multi-channel RF coils and a method for unwrapping phase/frequency maps that takes advantage of the information on phase evolution as a function of gradient echo time in GEPCI echo train.

Keywords

MRI; GEPCI; SWI; multi-contrast MRI; FLAIR; T2*; phase; phase unwrapping; multi-channel coil

Corresponding Author: Dmitriy A. Yablonskiy, PhD Mallinckrodt Institute of Radiology 4525 Scott Ave, Room 3216 St. Louis, MO 63110 Phone: 314-362-1815 FAX: 314-362-0526 YablonskiyD@wustl.edu http://bmr.wustl.edu/~dmitriy/.

Introduction

Gradient Recalled Echo (GRE) based MR imaging techniques have wide applications in MRI. Due to the absence of refocusing RF pulses GRE sequences are fast (for example FLASH (Haase *et al.* 1986)), and since low flip angles are usually applied, GRE sequences have low specific absorption rate, hence are particularly well suited for high field MRI. While MR signal generated from GRE techniques is complex, most traditional applications rely only on magnitude information whereas the phase information from the data is usually discarded. However, certain newer applications also rely on phase data. Among these, Susceptibility Weighted Imaging (SWI) (Haacke *et al.* 2009; Reichenbach *et al.* 1997) uses a specific algorithm based on GRE T2* weighted magnitude and phase data to create images sensitive to variations in tissue magnetic susceptibility resulting from sources such as venous blood, calcification, hemorrhage, iron stores, etc (Haacke *et al.* 2005; Haacke *et al.* 2009; Mittal *et al.* 2009; Ogg *et al.* 1999; Petridou *et al.* 2010; Reichenbach *et al.* 1997; Sedlacik *et al.* 2008). The clinical applications for SWI continue to expand steadily (Haacke 2011). Other techniques, some of which rely exclusively on the phase data of the GRE signal have also been intensely explored for uniquely characterizing anatomical structures that are especially evident at high field MRI (Duyn *et al.* 2007; Marques *et al.* 2009; Rauscher *et al.* 2005; Zhong *et al.* 2008), and even for creating maps of tissue magnetic susceptibility – the so called Quantitative Susceptibility Mapping (QSM) (de Rochefort *et al.* 2008; de Rochefort *et al.* 2010; Liu 2010; Liu *et al.* 2010; Schweser *et al.* 2010; Schweser *et al.* 2011; Shmueli *et al.* 2009). The information obtained from these techniques reveals image features complimentary to that obtained from traditional magnitude-based imaging and could improve our understanding of both normal tissue anatomy as well as changes in tissue in various pathological conditions. Importantly, the phase images are sensitive to various sources: susceptibility effects that are determined by variations in tissue composition (amount of proteins, lipids, iron, etc...) (Duyn *et al.* 2007; Fukunaga *et al.* 2010; He and Yablonskiy 2009), tissue micro architecture at the cellular and sub-cellular levels that alters relationship between tissue magnetic susceptibility and signal frequency/phase (He and Yablonskiy 2009); possible dependence of tissue magnetic susceptibility on orientation with respect to the magnetic field B0 (Lee *et al.* 2010; Liu 2010); frequency shifts that are induced by water-macromolecule exchange in the tissue (Luo *et al.* 2010; Shmueli *et al.* 2011; Zhong *et al.* 2008); and global shape of the object (Chu *et al.* 1990).

In addition to most commonly used GRE techniques with a single gradient echo, different versions of multi gradient echo sequences have also been used in MRI for multiple purposes. Ma and Wehrli (Ma and Wehrli 1996) proposed GESFIDE (Gradient Echo sampling of FID and spin Echo) sequence for separation of irreversible (R2) and reversible (R2') contributions to transverse signal decay rate constant R2*=R2+R2'. Another version of multi gradient echo sequence – GESSE (Gradient Echo Sampling of Spin Echo) was used for measuring tissue T2 relaxation (Cox and Gowland 2010; Yablonskiy and Haacke 1997), anisotropic properties of trabecular bone (Yablonskiy *et al.* 1997), and even tissue hemodynamic properties such for example as Oxygen Extraction Fraction and concentration of deoxyhemoglobin in blood vessel network (He and Yablonskiy 2007; He *et al.* 2008; Yablonskiy 1998). Multi gradient echo sequences were also frequently used for mapping brain tissue T2* (e.g. recent publications (Bender and Klose 2010; Lee *et al.* 2011) and references therein) and were proposed as a tool for mapping brain tissue myelin content (Du *et al.* 2007; Hwang *et al.* 2010). This list of course is not supposed to be inclusive. GEPCI – Gradient Echo Plural Contrast Imaging is a post-processing technique that based on the data collected from GRE sequence with multiple gradient echoes, allows simultaneous generation of naturally co-registered T2* (or R2*=1/T2*) maps, T1 weighted (T1w) or spin density images and frequency (or phase) maps from the same acquisition. It was proposed in (Bashir and Yablonskiy 2006; Yablonskiy 2000; Yablonskiy 2003) and successfully applied for

quantifying tissue damage in multiple sclerosis (Sati *et al.* 2010). In this study, we demonstrate that by combining the basic GEPCI images, we can also generate a number of additional (derived) images, such as (a) SWI-like images that are similar in contrast to standard SWI images, (b) GEPCI-SWI images that are SWI free of T1w contamination and RF field inhomogeneities, (c) T1f anatomical images with improved grey matter (GM) white matter (WM) contrast, (d) Fluid Suppressed T2* (FST2*) images that utilize GEPCI T1 data to suppress bright CSF signal in T2* maps providing a contrast in many ways similar to FLAIR T2 weighted images, and (e) SWI-T2* images that combine SWI contrast with quantitative T2* map and offer advantages of visualizing venous structure with hyperintense T2* lesions (e.g. MS lesions). While most of these and similar images have been used in MRI previously, herein we report for the first time a method that generates all of them from a single MRI scan. To analyze GEPCI images we use an improved algorithm for combining data from multi-channel RF coils and a method for unwrapping phase/frequency maps that takes advantage of the information on phase evolution as a function of gradient echo time in GEPCI echo train.

Materials and Methods

Acquisition

Brain images were collected from 5 healthy volunteers and one subject with Relapsing-Remitting MS who underwent brain MRI studies on a Siemens 3T Trio MRI scanner (Siemens, Erlangen, Germany). A 12-Channel phased-array head coil was used to obtain a 3D version of the multi gradient echo sequence with a resolution of 1×1×2 mm^3 or 1×1×3 mm^3, FOV of 256 mm × 192 mm and 11 gradient echoes (TR = 50 ms; minTE = 4 ms; delta-TE = 4 ms; bandwidth = 510Hz/Pixel; FA = 30°). Further effective resolution enhancement was achieved with zero-filling in k-space. Standard SWI images were also acquired with the same resolution and TR=27 ms, TE=20 ms, bandwidth 120Hz/Pixel, FA=15° for healthy volunteers; and standard FLAIR images were acquired for the MS patient with resolution 1.3×0.9×3 mm^3 by turbo spin echo sequence: TR=10 s, TI=2600 ms, TE=82 ms, turbo factor = 13, Echo trains per slice = 15. All studies were conducted with the approval of Washington University IRB.

Multi-channel data processing

Multi-channel data were combined using a generalization of previously developed algorithm (Quirk *et al.* 2009) that allows for the optimal estimation of quantitative parameters, such as MR signal decay rate constants. In original implementation it was assumed that the data from different channels are already phased coherently. Applying this algorithm for multi-gradient echo signal obtained from an *M*-channel RF coil, we get the following result:

$$S_{comb}(TE_n) = \frac{1}{M}\sum_{m=1}^{M} \lambda_m S_m(TE_1)\, S_m(TE_n) \tag{1}$$

where index *n* enumerates gradient echoes, index *m* enumerates RF channels, $S_{comb}(TE_n)$ is a combined signal corresponding to the gradient echo time TE_n, $S_m(TE_n)$ are signals from individual channels, and parameter λ_m is

$$\lambda_m = \frac{\frac{1}{M}\sum_{m'=1}^{M} \sigma^2_{m'}}{\sigma^2_m} \tag{2}$$

Here σ_m are noise amplitudes (r.m.s.) in corresponding channels (m). They are calculated by averaging data from 10×10 pixel area in the corner of magnitude images $|S_m(TE_n)|$. Since noise levels of each acquisition (echo times) are similar, they are subsequently averaged to obtain σ_m for a single channel. The Rician nature of noise in magnitude images does not affect estimate of parameters λ_m since they are ratios of σ_m^2. The parameters λ_m provide additional signal weighting and reduce contribution of RF channels with high noise level.

Generalizing this consideration for complex data leads to the following algorithm for data combination:

$$S_{comb}(TE_n) = \frac{1}{M}\sum_{m=1}^{M} \lambda_m \overline{S}_m(TE_1)\, S_m(TE_n) \tag{3}$$

where $\overline{S}_m(TE_1)$ is a complex conjugate of the signal from channel m at the first gradient echo time TE_1. Since signal phases of different channels differ by their initial values φ_{0m} but have the same frequency f, as described in

$$\varphi_m(TE_n) = \varphi_{0m} + 2\pi f \cdot TE_n \tag{4}$$

this procedure removes destructive interference of data due to the term φ_{0m} from multiple channels. The procedure described by Eq. (3) is applied to each voxel in the image.

Generating basic GEPCI images

Combined data are analyzed assuming mono-exponential signal decay and taking into account Eqs. (3) and (4):

$$S_{comb}(TE_n) = S_0^2 \cdot e^{-R_2^*(TE_n + TE_1)} \cdot e^{i2\pi f(TE_n - TE_1)} \tag{5}$$

Before fitting Eq. (5) to complex data (magnitude and phase images), the phase data were unwrapped for each voxel in a time domain using 11 data points (TE_n). If the frequency for some areas is high enough to cause multiple phase wraps within delta TE (that is 250Hz for our delta TE of 4 ms), then after time domain unwrapping there will be isolated areas in the frequency map that should be further unwrapped in spatial domain. Though most parts of the brain frequency map gets unwrapped already after the time domain procedure. The fitting procedure produces three naturally co-registered basic GEPCI images: a quantitative R2*=1/T2* map, a T1-weigted (S_0) image and a frequency (f) map. The frequency maps are then subsequently high-pass filtered to remove effects of macroscopic field inhomogeneities. Herein we use a 7×7 (out of 256×256) averaging matrix.

Generating secondary derived GEPCI images

Several *derived* images can also be generated based on these basic GEPCI images. First, a positive Frequency contrast Mask (FM) is created by setting negative frequency values to unity, and normalizing positive frequency values to be ranged from 0 to 1, such that 1 corresponds to zero frequency and 0 corresponds to highest frequency. This procedure is similar to creating phase masks in standard SWI procedure (Reichenbach *et al.* 1997).

SWI-like images are generated using the following equation

Here the T1 weighted image S_0 is T2* weighted with a certain TE (we used TE=20ms, which is typical echo time used for the SWI sequence on 3T systems) and is multiplied 4 times by the frequency mask (FM), which generates an image that mimics the standard SWI contrast (Reichenbach *et al.* 1997).

$$S_{SWI-like}(TE) = S_0 \cdot e^{-R2^* \cdot TE} \cdot FM^4 \quad (6)$$

GEPCI-SWI images are generated as follows

GEPCI-SWI images are free from T1 contrast contamination characteristic to the standard SWI because they are generated using pure T2* weighting and phase contrast without S_0 term. Here we also use TE=20ms and multiply the magnitude image 4 times with a frequency mask just as in original SWI (Reichenbach *et al.* 1997).

$$S_{GEPCI-SWI}(TE) = e^{-R2^* \cdot TE} \cdot FM^4 \quad (7)$$

Minimum intensity projection (minIP) images using seven slices were also calculated for both the SWI-like and the GEPCI-SWI images.

GEPCI-T1f images are derived by using only T1-weighted image (S0) and frequency contrast mask:

$$S_{GEPCI-T1F} = S_0 \cdot FM^4 \quad (8)$$

In these images GM/WM contrast is enhanced.

The goal here is to produce FST2* images that are T2* images with suppressed CSF signal that would “look similar” to FLAIR (fluid attenuated inversion recovery) T2 weighted images. Standard FLAIR-T2 images are obtained by using a long inversion pulse that suppresses the signal from CSF (long T1 component), and a long TE that produces heavy T2 weighting (Hajnal *et al.* 1992). To produce FST2* images we create a CSF mask (M_{CSF}) using the T1-weighted image (S0). The S0 image is first processed by FMRIB's Automated Segmentation Tool (FAST) (Smith *et al.* 2004; Woolrich *et al.* 2009; Zhang *et al.* 2001) to remove the bias in image intensity caused by RF field inhomogeneities. Example of the distribution of the corrected S0 values (T1w image) is plotted in a histogram, Fig. 1; the signal intensities are ranked as S(WM)>S(GM)>S(CSF), thus highest peak on the right corresponds to WM. Gaussian fitting was done on the right half of the main peak in this histogram determining peak position, X0, and standard deviation, STD. This allows thresholding of CSF signal. In this paper voxels that have S_0 values that are bigger than (X0 – 1.96 * STD) were considered as non-CSF area and their values were set as unity in M_{CSF} mask. Voxels with intensity below (X0 – 1.96 * STD) were normalized from 0 to 1, so that the darkest-appearing voxels on T1w image is 0, and brightest-apprearing voxels (those that are close to gray matter) is 1. The FST2* images are produced by multiplying the T2* map with the CSF mask *n* times.

$$S_{FST2^*} = T2^* \cdot M_{CSF}^n \quad (9)$$

Since the voxels that are set to 1 in the mask will not get much attenuation in the resulting image, the threshold should be selected within the grey matter area to achieve a better suppression of CSF signal. In this manuscript we have compared several choices of parameter n (1~4). The optimal choice of threshold and ‘n’ is subject to further discussion. These images look like FLAIR images in the way that they have essentially T2* contrast (similar to T2 weighting) with strongly attenuated CSF signal.

T2*-SWI Images—In some applications like multiple sclerosis (MS) it might be advantageous to generate images that simultaneously show venous structure and T2

hyperintense lesions (Grabner *et al.* 2011). Using GEPCI, this can be achieved by combining GEPCI-SWI and GEPCI FST2* images. Indeed, GEPCI-SWI data shows veins as dark contrast but are insensitive to hyperintense lesions. On the other hand, T2 hyperintense lesions are also hyperintense on FST2* images. We found that good visualization of the combined distribution of T2 hyperintense lesions and veins (and possible iron deposition) is achieved by multiplication of FST2* and GEPCI-SWI images so that T2 hyperintense lesions are contrasted by hypointense veins running through:

$$S_{FST2^*-SWI} = S_{FST2^*} \cdot S_{GEPCI-SWI} \tag{10}$$

It can also be applied to assess vascularity of tumors where tumors are bright on FST2*, and vascular structures inside tumors are dark.

Results and Discussions

T1 and T2* relaxation as well as phase evolution of MR signal are three independent physical phemomena which generate different soft tissue contrasts during MR imaging. Any conventional snapshot of Gradient-Echo images usually displays a mixture of these contrasts, although different sequence parameters can be chosen to enhance one or the other, at the cost of scanner time. GEPCI technique allows obtaining image data sets with multiple contrasts simutaneously. Moreover, since these different data sets are already co-registered, they can be combined in a variety of ways to generate images with novel contrast properties. It is also important to emphasize that since all GEPCI images – basic and derived - are naturally co-registered, it simplifies data analysis between multiple contrast mechanisms.

Multi-channel data processing and phase unwrapping

In order to generate GEPCI images, data from multi-channel RF coil should first be combined in a single data set. Figure 2 demonstrates the phase unwrapping and channel combination procedure proposed in this manuscript (see detail description in the Methods section). From phase maps shown in the top two rows of Fig. 2, we can see that combining phase images from different channels requires solving two problems. First, individual receivers have different phase offsets, as described in Eq.(4). To address this issue,for each voxel we multiplied signal from each channel by the complex conjugate of data from the first echo of the corresponding channel, thus eliminating the phase offsets of each receiver coil. Data from all channels were then averaged with their sensitivity weighting per Eq.(3) to achieve optimal SNR with minimum error in parameters estimate (Quirk *et al.* 2009). Second problem is that phase images are affected by ‘wraps’, where jumps of 2π happen between adjacent voxels due to phase values of $2\pi m + \theta$ (m is integer) are encoded as identical. This problem becomes more pronounced at longer echo times. Usually phase unwrapping is accomplished in the image domain, where different algorithms have been used (see for example (Hammond *et al.* 2008; Witoszynskyj *et al.* 2009)). Here we take advantage of having gradient echoes corresponding to multiple TE and unwrap signal phase in the time domain for each imaging voxel. Frequency maps were then generated by fitting phase data for each voxel as function of the gradient echo times per Eq. (4). Note that difference in wrapping pattern in the phase image corresponding to different TE does not affect this fitting procedure and resultant frequency maps. Though for areas of the brain with strong field inhomogeneities additional unwrapping of the frequency map in the image domain might be required, this was not the case in any of our data.

Basic GEPCI images—Example of basic GEPCI images is shown in Fig. 3. The frequency map presents significantly different contrast from the corresponding magnitude image (T1w) or the R2* map. White matter (WM) showed up darker than the cortex and caudate, putamen in the deep grey matter area on frequency map; this contrast is reversed on

T1w image; on the R2* map however, WM showed up darker than the caudate and putamen, although still brighter than the cortex region. The nature of WM "darkness" on phase images was explained in (He and Yablonskiy 2009) based on the introduced there Generalized Lorentzian approach. According to this theory, the longitudinal structures (myelin sheaths, axons, neurofilaments, etc.) that comprise WM do not contribute to the total frequency shift for the circular cylindrical axonal tracts even though WM has higher magnetic susceptibility than the GM. The frequency map allows superior delineation of the caudate, internal capsule, pallidum and putamen, whereas the differentiation is not as clear on T1 weighted image or R2* map. Grey matter/White matter boundaries are also clearly depicted on frequency maps. These results are similar to previously reported with high field MRI (Duyn *et al.* 2007).

GEPCI-SWI and SWI-like Images—In this study, by combining basic GEPCI data sets in a manner analogous to standard SWI approach, we generated SWI like images and compared them to the Siemens scanner generated SWI data (Figs. 4A and 4B). The images resulting from the standard SWI sequence were as usually contaminated by T1-weighting. This remains the case when GRE with several gradient echoes is used, although multi gradient echo approach allows increasing the signal to noise ratio (SNR) and contrast to noise ratio (CNR) of brain SWI images (Denk and Rauscher 2010). The most obvious consequence of this T1 contamination is the 'dark CSF' area, particularly in the mIP images, which reduces contrast between the veins and CSF (Fig. 4A and 4B). One way to resolve this issue was suggested by Haacke et al (Haacke *et al.* 2009), that is to use small flip angles to minimize darkening of CSF area. Imaging parameter on 3.0T MRI scanner was proposed: FA 12-17 degrees, TR 25-35 ms, TE 20 ms, BW 80-100 Hz/pixel. As our images showed, although imaging parameters we used for the standard SWI imaging is within the recommended range, additional adjustments shall be made to get desirable SWI contrast. Further, using small flip angle to minimize darkening of CSF area will inevitably result in loss of grey white contrast on the SWI images.

Using GEPCI approach allows overcoming this problem without losing signal. Indeed, GEPCI data were acquired with imaging parameters that maximize the T1-weighted contrast for S(0) as well as preserving SNR characteristic for optimal flip angle. In contrast to the SWI–like images and the standard scanner generated SWI images, GEPCI-SWI images had preserved bright CSF signal as well as preserved GM/WM contrast. This phenomenon maybe particularly useful in characterizing the deep veins in the area of the lateral ventricles. Such information about the deep veins is likely to be useful in surgical planning for patients who are set to undergo procedures such as placement of deep brain stimulators (Binder *et al.* 2003). Note that, the GEPCI-SWI image is as sharp as or even sharper than conventional SWI images with regard to vessel delineation. Also note that the GEPCI-SWI significantly enhances the gray and white matter interfaces, as seen in Fig. 4.

GEPCI-T1f Images—Another novel combination of the GEPCI basic images incorporates the frequency map and the T1-weighting (S0). The grey matter area on T1-weighted images is darker than white matter. Considering the fact that grey matter tends to present more positive frequencies in frequency maps than white matter, plus the transition between gray and white matter on frequency map is more sharply delineated, we explored enhancement of GM/WM contrast by multiplication of the GEPCI T1w image with the frequency mask. The Resulting images (Fig. 5) did indeed demonstrate more crisp GM/WM borders as well as enhanced GM/WM contrast compared to the T1w images. Deep grey matter structures such as caudate and putamen nuclei are also clearly outlined on the GEPCI-T1f images. These images are likely to be very useful in detecting malformations of cortical development in patients with intractable epilepsy, since they are more likely to be sensitive to blurring of the GM/WM interface from subtle cortical migrational abnormalities (Kanekar and Gent 2011).

Multiple sclerosis lesions in cortex, typically not clearly resolved by standard MRI (Pirko *et al.* 2007), might be more clearly seen. Additionally, these images also offer a promising new method to achieve GM/WM segmentation which will result in more accurate volumetric data as well as improve data from cerebral perfusion studies.

FST2* Images—Example of GEPCI FST2* image is shown in Fig. 6. These images are similar to FLAIR images in the way that CSF is suppressed based on tissue T1 properties. However, unlike T2 weighted FLAIR images which are based on T2 weighting, FST2* image is based on T2* map. Since difference between T2 and T2* values is usually small, especially in well shimmed white matter areas (He and Yablonskiy 2007) FST2* images could be used to detect T2 sensitive changes in the brain, such as visualizing edema, hyperintense lesions (in multiple sclerosis (Sati *et al.* 2010)), cerebral infarctions, which are usually well detected on the FLAIR sequences. Various degree of fluid suppression has been shown in Fig.6, as we go from n=1 to n=4. Choice may be made for different applications. For example, in MS brain part of the MS lesions can be suppressed together with CSF signal when bigger 'n' is applied. We could choose n=1 in order to maintain hyper-intensity of the lesions. Or since MS lesions are likely to appear in white matter areas, we could avoid suppression of lesions by designing WM masks based on GEPCI-T1w images. Additionally, based on its quantitative T2* nature, it could also be used to detect T2* sensitive changes, such as microbleeds or microcalcifications in the brain. Indeed, the fluid suppression based on the GEPCI-T1w image will not suppress artery signals on the T2* map, yet it should not affect most brain area.

Possible applications of GEPCI in Clinical Arena

GEPCI in MS

GEPCI technique could also be applied to monitoring patients with multiple sclerosis. Typical MRI protocol for detecting MS includes FLAIR (fluid-attenuated inversion recovery), T2-weighted spin-echo, and T1-weighted spin-echo (including with and without Gd-enhancement) (Keegan and Noseworthy 2002; McFarland 2009). Phase imaging and susceptibility weighted imaging has also been proposed for identification of MS lesions (Haacke *et al.* 2009; Hammond *et al.* 2008). While typical MRI protocol aims at imaging the contrast due to variations in the tissue characteristic relaxation rates, which are likely to represent lesions that are the result of myelin and/or axonal loss, or inflammation, the SWI and phase imaging are able to visualize small veins within white matter, which might help resolve the timing of interactions between venous structures and MS lesions. With the whole set of GEPCI images, as shown in Fig. 7, we can obtain information on both the MS lesions and white matter veins within a single acquisition.

MS lesions are identified as hypointense on GEPCI-T1w image (Fig. 7a), and hyperintense on FST2* (Fig. 6) due to increased T1 and T2* relaxation times. The T2* values in the lesion area could be further used for more quantitative assessment of MS lesions (Sati *et al.* 2010). GEPCI-SWI image (Fig. 7d) shows veins without apparent indication of lesions. Lesions that are slightly hyperintense on frequency maps are darkened on T1f (Fig. 7c) compared to T1weighted image (Fig. 7a). Veins also appeared on T1f image because of frequency map. Thus visualization of the distribution of lesions and their relation to veins (and possible iron deposition) is achieved by multiplication of FST2* and GEPCI-SWI images (Fig. 6 with n=4 and Fig. 7d), so that hyperintense lesions are contrasted by dark veins running through. This idea is similar to that recently proposed in (Grabner *et al.* 2011) who combined FLAIR images acquired at 3.0 T and SWI acquired at 7.0 T. However, with GEPCI images, we easily achieve similar contrast from a single acquisition and complete, intrinsic co-registration. Comparing Fig.7e and 7f, lesions that are hyperintense on standard FLAIR images are also clearly seen on the fusion of FST2* and SWI image where veins

associated with MS lesions are readily observed. However, not all lesions in Fig. 7 are associated with veins (e.g. green arrow on Fig.7e and 7f), and the underlying relationship between veins and pathology of MS remains to be investigated.

Other Possible Applications—The advantage of having a battery of images with multiple contrasts can have advantages for numerous clinical applications. For example, combining GEPCI-SWI and GEPCI-T1f images, can potentially be used to correct for venous contamination in dynamic susceptibility contrast MR perfusion maps such as obtained in stroke patients (Reishofer *et al.* 2007). In some patients, cavernous malformations can be associated with epilepsy. With co-localized both SWI and T1f contrasts (venous and GM/WM delineation), it is possible to visualize the cavernous malformation and also evaluate its relationship to the adjacent cerebral cortex. This may provide new insights into the mechanism of epileptogensis in these patients and allow for better surgical planning (Maciunas *et al.* 2010; Menzler *et al.* 2011). This combined contrast could also be useful in co-localizing subtle cortical malformations which may be found in the vicinity of complex venous abnormalities in some patients with epilepsy. The preservation of cortical GM/WM detail and representation of venous anatomy is also likely to be useful in surgical planning in patients with brain tumors who are set to undergo biopsies or curative resections (Barkovich 1988; Desai *et al.* 2002). Based on these images, the surgeon will be better able to avoid prominent veins at the tumor margins as well as estimate the relationship of the tumor resection margins to eloquent areas of the cerebral cortex at the same time.

Although a number of novel contrast mechanisms have been highlighted in this manuscript, several limitations of the present study must also be mentioned. Most importantly, in this manuscript we have not discussed issues related to magnetic field inhomogeneities and their influence on quantitative results obtained with GEPCI technique, especially on quantitative evaluation of T2* relaxation time constant. Influences of field inhomogeneities are particularly significant around the tissue/bone or tissue/air interfaces such as sinuses, ear canals, etc. However, away from these areas and for high resolution imaging as was used herein, this issue creates only minor problems in most parts of the brain. Detailed discussions of these issues can be found elsewhere (see for example (Fernandez-Seara and Wehrli 2000; Yablonskiy 1998; Yablonskiy and Haacke 1994)) and will also be addressed in our future publications.

The role of field inhomogeneities should also be noted when interpreting the derived contrasts based on application of the frequency masks, FM. This means, masked images are strongly influenced by the quality of FM, especially when high pass filtering is not properly removing macroscopic field inhomogeneity (eg. edge of the brain). In fact, GEPCI-SWI in Fig.4A-c and Fig.4B-c, the edge of the brain shows hypointensity. Application of recently proposed advanced phase processing methods, e.g. SHARP method (Schweser *et al.* 2011) or the projection onto dipole fields (Liu *et al.* 2011), could result in a more accurate removing of the artifacts related to macroscopic field inhomogeneities. Other examples would be sharp transitions in susceptibility of the brain tissue such as deep nuclei or ventricles. One might notice that the structures in frequency map are not always the same as that in magnitude images. In such cases tissue magnetic susceptibility will affect frequency map not only at the location of susceptibility variations but also in the surrounding areas. One of the ways to deal with this problem is already mentioned in the introduction quantitative susceptibility mapping (de Rochefort *et al.* 2008; de Rochefort *et al.* 2010; Liu *et al.* 2010; Schweser *et al.* 2010; Schweser *et al.* 2011; Shmueli *et al.* 2009).

Another potential area of improvement includes accounting for the multi-compartment tissue structure. Quantification of myelin-bound and free water fractions by a

multiexponential analysis of the T2 decay has been discussed (Beaulieu *et al.* 1998; Mackay *et al.* 1994). Signal obtained based on a Carr-Purcell-Meiboom-Gill (CPMG) or Turbo Spin-Echo (TSE) sequence with multiple TEs was modeled by three pool model (Lancaster *et al.* 2003), or four pool model (Levesque and Pike 2009), or by non-negative least squares (Whittall and Mackay 1989). Recently, it has been shown that T2* decay, which is measured by multi-echo gradient echo sequence, could also be used for extraction of myelin water fraction (Du *et al.* 2007; Hwang *et al.* 2010). However these issues are beyond the scope of the current manuscript.

In Conclusion

The GEPCI technique based on post processing of the multi-echo GRE data produces high quality frequency maps, high resolution R2* maps and T1-weighted images. These data sets can then be combined in novel ways to produce high resolution images which can offer excellent depiction of the intracranial venous system (SWI like and GEPCI-SWI images), images which promise to significantly improve the delineation of cerebral grey and white matter interfaces (GEPCI-T1f images) and GEPCI-FST2* images that look similar to FLAIR images. These novel imaging data sets can potentially find clinical applications in studying a variety of common neurological disorders. They can also find applications in basic neuro-anatomical and neuropathological research. Most importantly, these images with novel contrast properties can be obtained without any increase in acquisition time, and they are naturally co-registered obviating additional costs in terms of scanner time and personnel.

Acknowledgments

We would like to thank Dr. Joseph Ackerman for helpful discussion, volunteers for their time, Mark Nolte, Scott Love, and Glenn Foster for helping with MRI scanning. This publication was supported by NIH grants R01 NS055963, UL1 RR024992, U.S. Department of Defense MS090031, and Imaging Sciences Pathway fellowship funded by NIH grant 5T90 DA022781.

References

Barkovich AJ. Abnormal Vascular Drainage in Anomalies of Neuronal Migration. American Journal of Neuroradiology. 1988; 9(5):939–942. [PubMed: 3140639]

Bashir, A.; Yablonskiy, DA. Gradient Echo Plural Contrast Imaging (GEPCI).. Annual Meeting of the International Society for Magnetic Resonance in Medicine; Seattle, Washington. 2006.

Beaulieu C, Fenrich FR, Allen PS. Multicomponent water proton transverse relaxation and T-2-discriminated water diffusion in myelinated and nonmyelinated nerve. Magnetic Resonance Imaging. 1998; 16(10):1201–1210. [PubMed: 9858277]

Bender B, Klose U. The in vivo influence of white matter fiber orientation towards B(0) on T2* in the human brain. NMR Biomed. 2010; 23(9):1071–1076. [PubMed: 20665897]

Binder DK, Rau G, Starr PA. Hemorrhagic complications of microelectrode-guided deep brain stimulation. Stereotactic and Functional Neurosurgery. 2003; 80(1-4):28–31. [PubMed: 14745205]

Chu SCK, Xu Y, Balschi JA, Springer CS. Bulk Magnetic-Susceptibility Shifts in Nmr-Studies of Compartmentalized Samples - Use of Paramagnetic Reagents. Magnetic Resonance in Medicine. 1990; 13(2):239–262. [PubMed: 2156125]

Cox EF, Gowland PA. Simultaneous Quantification of T(2) and T(2)' Using a Combined Gradient Echo-Spin Echo Sequence at Ultrahigh Field. Magnetic Resonance in Medicine. 2010; 64(5):1441–1446.

de Rochefort L, Brown R, Prince MR, Wang Y. Quantitative MR susceptibility mapping using piece-wise constant regularized inversion of the magnetic field. Magnetic Resonance in Medicine. 2008; 60(4):1003–1009. [PubMed: 18816834]

de Rochefort L, Liu T, Kressler B, Liu J, Spincemaille P, Lebon V, Wu JL, Wang Y. Quantitative Susceptibility Map Reconstruction from MR Phase Data Using Bayesian Regularization: Validation

and Application to Brain Imaging. Magnetic Resonance in Medicine. 2010; 63(1):194–206. [PubMed: 19953507]

Denk C, Rauscher A. Susceptibility Weighted Imaging With Multiple Echoes. Journal of Magnetic Resonance Imaging. 2010; 31(1):185–191. [PubMed: 20027586]

Desai K, Bhayani R, Nadkarni T, Limaye U, Goel A. Developmental deep venous system anomaly associated with congenital malformation of the brain. Pediatric Neurosurgery. 2002; 36(1):37–39. [PubMed: 11818745]

Du YP, Chu R, Hwang D, Brown MS, Kleinschmidt-DeMasters BK, Singel D, Simon JH. Fast multislice mapping of the myelin water fraction using multicompartment analysis of T-2* decay at 3T: A preliminary postmortem study. Magnetic Resonance in Medicine. 2007; 58(5):865–870. [PubMed: 17969125]

Duyn JH, van Gelderen P, Li TQ, de Zwart JA, Koretsky AP, Fukunaga M. High-field MRI of brain cortical substructure based on signal phase. Proceedings of the National Academy of Sciences of the United States of America. 2007; 104(28):11796–11801. [PubMed: 17586684]

Fernandez-Seara MA, Wehrli FW. Postprocessing technique to correct for background gradients in image-based R-2(*) measurements. Magnetic Resonance in Medicine. 2000; 44(3):358–366. [PubMed: 10975885]

Fukunaga M, Li TQ, van Gelderen P, de Zwart JA, Shmueli K, Yao B, Lee J, Maric D, Aronova MA, Zhang GF, Leapman RD, Schenck JF, Merkle H, Duyn JH. Layer-specific variation of iron content in cerebral cortex as a source of MRI contrast. Proceedings of the National Academy of Sciences of the United States of America. 2010; 107(8):3834–3839. [PubMed: 20133720]

Grabner G, Dal-Bianco A, Schernthaner M, Vass K, Lassmann H, Trattnig S. Analysis of Multiple Sclerosis Lesions Using a Fusion of 3.0 T FLAIR and 7.0 T SWI Phase: FLAIR SWI. Journal of Magnetic Resonance Imaging. 2011; 33(3):543–549. [PubMed: 21563237]

Haacke EM, Cheng NY, House MJ, Liu Q, Neelavalli J, Ogg RJ, Khan A, Ayaz M, Kirsch W, Obenaus A. Imaging iron stores in the brain using magnetic resonance imaging. Magn Reson Imaging. 2005; 23(1):1–25. [PubMed: 15733784]

Haacke EM, Makki M, Ge YL, Maheshwari M, Sehgal V, Hu JN, Selvan M, Wu Z, Latif Z, Xuan Y, Khan O, Garbern J, Grossman RI. Characterizing Iron Deposition in Multiple Sclerosis Lesions Using Susceptibility Weighted Imaging. Journal of Magnetic Resonance Imaging. 2009; 29(3): 537–544. [PubMed: 19243035]

Haacke EM, Mittal S, Wu Z, Neelavalli J, Cheng YCN. Susceptibility-Weighted Imaging: Technical Aspects and Clinical Applications, Part 1. American Journal of Neuroradiology. 2009; 30(1):19–30. [PubMed: 19039041]

Haacke, EM.; Reichenbach, JR. Susceptibility Weighted Imaging in MRI: Basic Concepts and Clinical Applications. Wiley-Blackwell; 2011.

Haase A, Frahm J, Matthaei D, Hanicke W, Merboldt KD. Flash Imaging - Rapid Nmr Imaging Using Low Flip-Angle Pulses. Journal of Magnetic Resonance. 1986; 67(2):258–266.

Hajnal JV, Bryant DJ, Kasuboski L, Pattany PM, Decoene B, Lewis PD, Pennock JM, Oatridge A, Young IR, Bydder GM. Use of Fluid Attenuated Inversion Recovery (Flair) Pulse Sequences in Mri of the Brain. Journal of Computer Assisted Tomography. 1992; 16(6):841–844. [PubMed: 1430427]

Hammond KE, Lupo JM, Xu D, Metcalf M, Kelley DAC, Pelletier D, Chang SM, Mukherjee P, Vigneron DB, Nelson SJ. Development of a robust method for generating 7.0 T multichannel phase images of the brain with application to normal volunteers and patients with neurological diseases. Neuroimage. 2008; 39(4):1682–1692. [PubMed: 18096412]

Hammond KE, Metcalf M, Carvajal L, Okuda DT, Srinivasan R, Vigneron D, Nelson SJ, Pelletier D. Quantitative In Vivo Magnetic Resonance Imaging of Multiple Sclerosis at 7 Tesla with Sensitivity to Iron. Annals of Neurology. 2008; 64(6):707–713. [PubMed: 19107998]

He X, Yablonskiy DA. Quantitative BOLD: mapping of human cerebral deoxygenated blood volume and oxygen extraction fraction: default state. Magn Reson Med. 2007; 57(1):115–126. [PubMed: 17191227]

He X, Yablonskiy DA. Biophysical mechanisms of phase contrast in gradient echo MRI. Proceedings of the National Academy of Sciences of the United States of America. 2009; 106(32):13558–13563. [PubMed: 19628691]

He X, Zhu M, Yablonskiy DA. Validation of Oxygen Extraction Fraction Measurement by qBOLD Technique. Magn Reson Med. 2008; 60(4):882–888. [PubMed: 18816808]

Hwang D, Kim DH, Du YPP. In vivo multi-slice mapping of myelin water content using T-2* decay. Neuroimage. 2010; 52(1):198–204. [PubMed: 20398770]

Kanekar S, Gent M. Malformations of cortical development. Semin Ultrasound CT MR. 2011; 32(3): 211–227. [PubMed: 21596277]

Keegan BM, Noseworthy JH. Multiple sclerosis. Annual Review of Medicine. 2002; 53:285–302.

Lancaster JL, Andrews T, Hardies LJ, Dodd S, Fox PT. Three-pool model of white matter. Journal of Magnetic Resonance Imaging. 2003; 17(1):1–10. [PubMed: 12500269]

Lee J, Shmueli K, Fukunaga M, van Gelderen P, Merkle H, Silva AC, Duyn JH. Sensitivity of MRI resonance frequency to the orientation of brain tissue microstructure. Proceedings of the National Academy of Sciences of the United States of America. 2010; 107(11):5130–5135. [PubMed: 20202922]

Lee J, van Gelderen P, Kuo LW, Merkle H, Silva AC, Duyn JH. T(2)*-based fiber orientation mapping. Neuroimage. 2011; 57(1):225–234. [PubMed: 21549203]

Levesque IR, Pike GB. Characterizing Healthy and Diseased White Matter Using Quantitative Magnetization Transfer and Multicomponent T-2 Relaxometry: A Unified View via a Four-Pool Model. Magnetic Resonance in Medicine. 2009; 62(6):1487–1496. [PubMed: 19859946]

Liu C. Susceptibility tensor imaging. Magnetic Resonance in Medicine. 2010; 63(6):1471–1477. [PubMed: 20512849]

Liu T, Khalidov I, de Rochefort L, Spincemaille P, Liu J, Tsiouris AJ, Wang Y. A novel background field removal method for MRI using projection onto dipole fields (PDF). NMR Biomed. 2011; 24(9):1129–1136. [PubMed: 21387445]

Liu TA, Spincemaille P, de Rochefort L, Wong R, Prince M, Wang Y. Unambiguous identification of superparamagnetic iron oxide particles through quantitative susceptibility mapping of the nonlinear response to magnetic fields. Magnetic Resonance Imaging. 2010; 28(9):1383–1389. [PubMed: 20688448]

Luo J, He X, d'Avignon DA, Ackerman JJH, Yablonskiy DA. Protein-induced water H-1 MR frequency shifts: Contributions from magnetic susceptibility and exchange effects. Journal of Magnetic Resonance. 2010; 202(1):102–108. [PubMed: 19879785]

Ma JF, Wehrli FW. Method for image-based measurement of the reversible and irreversible contribution to the transverse-relaxation rate. Journal of Magnetic Resonance Series B. 1996; 111(1):61–69. [PubMed: 8620286]

Maciunas JA, Syed TU, Cohen ML, Werz MA, Maciunas RJ, Koubeissi MZ. Triple pathology in epilepsy: Coexistence of cavernous angiomas and cortical dysplasias with other lesions. Epilepsy Research. 2010; 91(1):106–110. [PubMed: 20674276]

Mackay A, Whittall K, Adler J, Li D, Paty D, Graeb D. In-Vivo Visualization of Myelin Water in Brain by Magnetic-Resonance. Magnetic Resonance in Medicine. 1994; 31(6):673–677. [PubMed: 8057820]

Marques JP, Maddage R, Mlynarik V, Gruetter R. On the origin of the MR image phase contrast: An in vivo MR microscopy study of the rat brain at 14.1 T. Neuroimage. 2009; 46(2):345–352. [PubMed: 19254768]

McFarland HF. Examination of the role of magnetic resonance imaging in multiple sclerosis: A problem-orientated approach. Annals of Indian Academy of Neurology. 2009; 12(4):254–263. [PubMed: 20182573]

Menzler K, Thiel P, Hermsen A, Chen X, Benes L, Miller D, Sure U, Knake S, Rosenow F. The role of underlying structural cause for epilepsy classification: Clinical features and prognosis in mesial temporal lobe epilepsy caused by hippocampal sclerosis versus cavernoma. Epilepsia. 2011; 52(4): 707–711. [PubMed: 21426322]

Mittal S, Wu Z, Neelavalli J, Haacke EM. Susceptibility-Weighted Imaging: Technical Aspects and Clinical Applications, Part 2. American Journal of Neuroradiology. 2009; 30(2):232–252. [PubMed: 19131406]

Ogg RJ, Langston JW, Haacke EM, Steen RG, Taylor JS. The correlation between phase shifts in gradient-echo MR images and regional brain iron concentration. Magn Reson Imaging. 1999; 17(8):1141–1148. [PubMed: 10499676]

Petridou N, Wharton SJ, Lotfipour A, Gowland P, Bowtell R. Investigating the effect of blood susceptibility on phase contrast in the human brain. Neuroimage. 2010; 50(2):491–498. [PubMed: 20026280]

Pirko I, Lucchinetti CF, Sriram S, Bakshi R. Gray matter involvement in multiple sclerosis. Neurology. 2007; 68(9):634–642. [PubMed: 17325269]

Quirk JD, Sukstanskii AL, Bretthorst GL, Yablonskiy DA. Optimal decay rate constant estimates from phased array data utilizing joint Bayesian analysis. Journal of Magnetic Resonance. 2009; 198(1): 49–56. [PubMed: 19181549]

Rauscher A, Sedlacik J, Barth M, Mentzel HJ, Reichenbach JR. Magnetic susceptibility-weighted MR phase imaging of the human brain. AJNR Am J Neuroradiol. 2005; 26(4):736–742. [PubMed: 15814914]

Reichenbach JR, Venkatesan R, Schillinger DJ, Kido DK, Haacke EM. Small vessels in the human brain: MR venography with deoxyhemoglobin as an intrinsic contrast agent. Radiology. 1997; 204(1):272–277. [PubMed: 9205259]

Reishofer G, Fazekas F, Keeling S, Enzinger C, Payer F, Simbrunner J, Stollberger R. Minimizing macrovessel signal in cerebral perfusion imaging using independent component analysis. Magnetic Resonance in Medicine. 2007; 57(2):278–288. [PubMed: 17260383]

Sati P, Cross AH, Luo J, Hildebolt CF, Yablonskiy DA. In vivo quantitative evaluation of brain tissue damage in multiple sclerosis using gradient echo plural contrast imaging technique. Neuroimage. 2010; 51(3):1089–1097. [PubMed: 20338247]

Schweser F, Deistung A, Lehr BW, Reichenbach JR. Differentiation between diamagnetic and paramagnetic cerebral lesions based on magnetic susceptibility mapping. Medical Physics. 2010; 37(10):5165–5178. [PubMed: 21089750]

Schweser F, Deistung A, Lehr BW, Reichenbach JR. Quantitative imaging of intrinsic magnetic tissue properties using MRI signal phase: an approach to in vivo brain iron metabolism? Neuroimage. 2011; 54(4):2789–2807. [PubMed: 21040794]

Sedlacik J, Kutschbach C, Rauscher A, Deistung A, Reichenbach JR. Investigation of the influence of carbon dioxide concentrations on cerebral physiology by susceptibility-weighted magnetic resonance imaging (SWI). Neuroimage. 2008; 43(1):36–43. [PubMed: 18678260]

Shmueli K, de Zwart JA, van Gelderen P, Li TQ, Dodd SJ, Duyn JH. Magnetic Susceptibility Mapping of Brain Tissue In Vivo Using MRI Phase Data. Magnetic Resonance in Medicine. 2009; 62(6): 1510–1522. [PubMed: 19859937]

Shmueli K, Dodd SJ, Li TQ, Duyn JH. The Contribution of Chemical Exchange to MRI Frequency Shifts in Brain Tissue. Magnetic Resonance in Medicine. 2011; 65(1):35–43. [PubMed: 20928888]

Smith SM, Jenkinson M, Woolrich MW, Beckmann CF, Behrens TEJ, Johansen-Berg H, Bannister PR, De Luca M, Drobnjak I, Flitney DE, Niazy RK, Saunders J, Vickers J, Zhang YY, De Stefano N, Brady JM, Matthews PM. Advances in functional and structural MR image analysis and implementation as FSL. Neuroimage. 2004; 23:S208–S219. [PubMed: 15501092]

Whittall KP, Mackay AL. Quantitative Interpretation of Nmr Relaxation Data. Journal of Magnetic Resonance. 1989; 84(1):134–152.

Witoszynskyj S, Rauscher A, Reichenbach JR, Barth M. Phase unwrapping of MR images using Phi UN - A fast and robust region growing algorithm. Medical Image Analysis. 2009; 13(2):257–268. [PubMed: 19070532]

Woolrich MW, Jbabdi S, Patenaude B, Chappell M, Makni S, Behrens T, Beckmann C, Jenkinson M, Smith SM. Bayesian analysis of neuroimaging data in FSL. Neuroimage. 2009; 45(1):S173–S186. [PubMed: 19059349]

Yablonskiy DA. Quantitation of intrinsic magnetic susceptibility-related effects in a tissue matrix. Phantom study. Magnetic Resonance in Medicine. 1998; 39(3):417–428. [PubMed: 9498598]

Yablonskiy, DA. Gradient echo plural contrast imaging (GEPCI) - New fast magnetic resonance imaging technique for simultaneous acquisition of T2, T1 (or spin density) and T2*-weighted images.. RSNA Annual Meeting 2000; Chicago, IL. 2000.

Yablonskiy, DA. T2 contrast in magnetic resonance imaging with gradient echoes.. 2003. US Patent 6,603,989

Yablonskiy DA, Haacke EM. Theory of Nmr Signal Behavior in Magnetically Inhomogeneous Tissues - the Static Dephasing Regime. Magnetic Resonance in Medicine. 1994; 32(6):749–763. [PubMed: 7869897]

Yablonskiy DA, Haacke EM. An MRI method for measuring T-2 in the presence of static and RF magnetic field inhomogeneities. Magnetic Resonance in Medicine. 1997; 37(6):872–876. [PubMed: 9178238]

Yablonskiy DA, Reinus WR, Stark H, Haacke EM. Quantitation of T-2' anisotropic effects on magnetic resonance bone mineral density measurement. Magnetic Resonance in Medicine. 1997; 37(2):214–221. [PubMed: 9001145]

Zhang YY, Brady M, Smith S. Segmentation of brain MR images through a hidden Markov random field model and the expectation-maximization algorithm. Ieee Transactions on Medical Imaging. 2001; 20(1):45–57. [PubMed: 11293691]

Zhong K, Leupold J, von Elverfeldt D, Speck O. The molecular basis for gray and white matter contrast in phase imaging. Neuroimage. 2008; 40(4):1561–1566. [PubMed: 18353683]

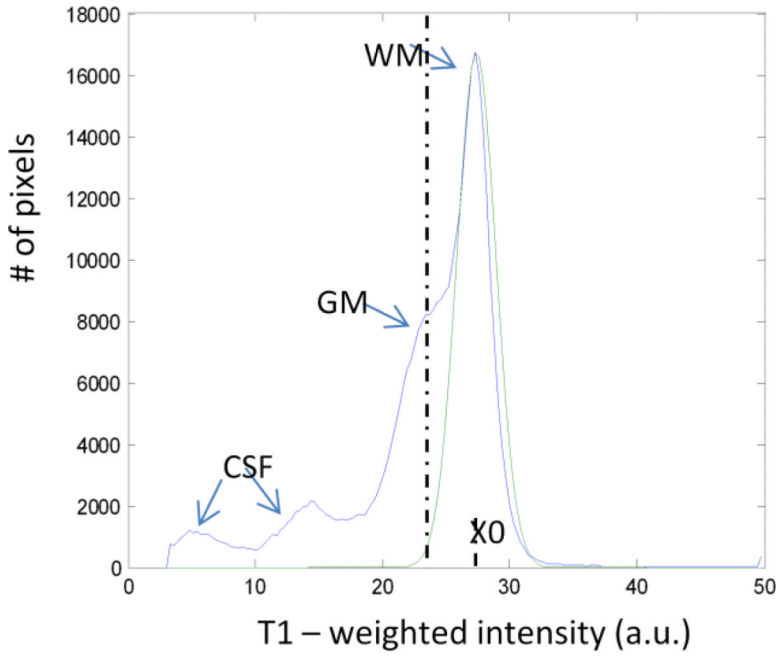

Figure 1.

An example of the histogram of GEPCI T1w image. Different brain tissue components are indicated on the histogram : white matter (WM), grey matter (GM), cerebrospinal fluid (CSF). X0 is the position of the WM peak. The vertical line indicates selected threshold that is used for CSF suppression in the FST2* images.

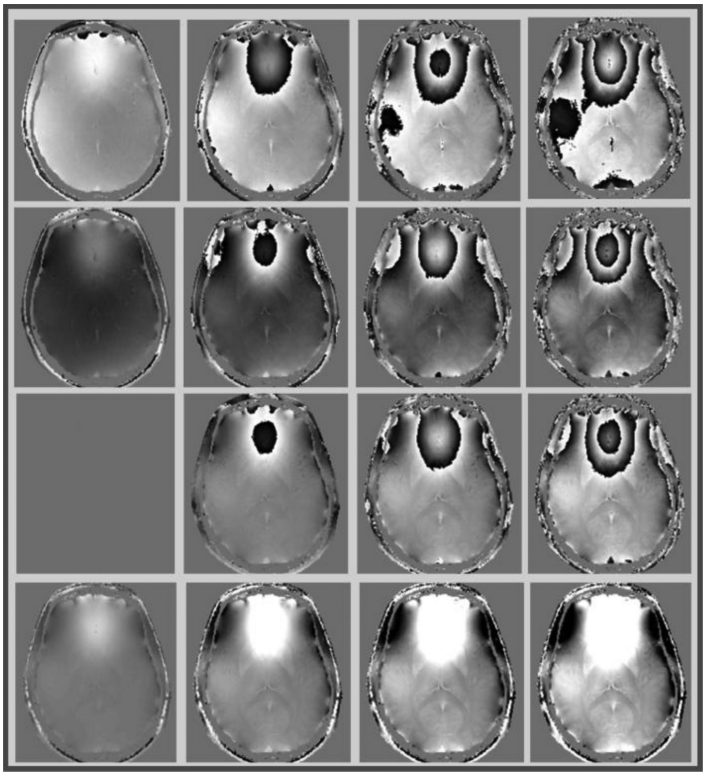

Figure 2.
Example of the phase images before and after channel combination procedure. Top two rows show phase images at TE equals 4 ms, 12 ms, 20 ms, 28 ms from 2 different channels; Third row shows combined phase images obtained after channel combination according to Eq. (3). First image in this row is zero because the phase of the first echo is compensated during channel combination. Bottom row shows phase images after unwrapping in the time domain as discussed in the methods section.

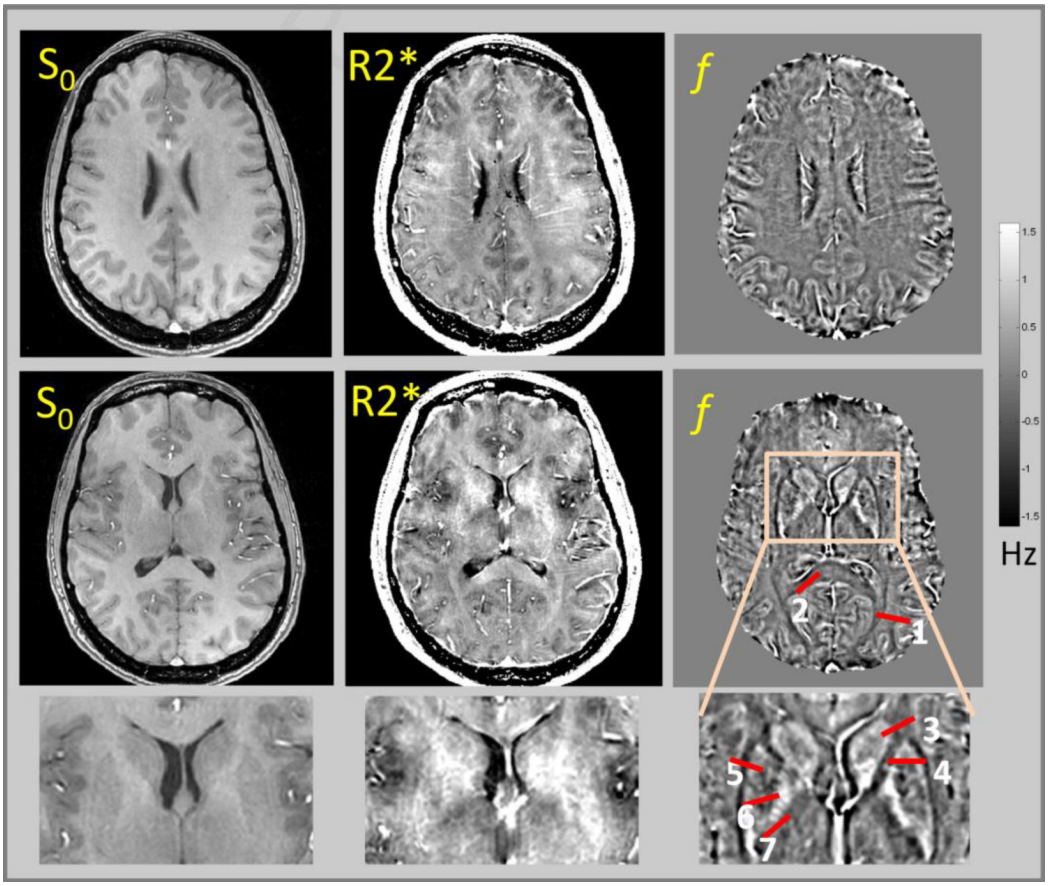

Figure 3.

Example the basic contrast images generated by GEPCI technique from two axial brain slices (first and second rows). Lower row shows detail picture of the part of the images identified by a square. As described in Eq.(5), S0 is the T1w image, R2* map is derived from the magnitude of the signal decay, and the third image is a frequency map (*f*). The scale bar shows distribution of frequencies. Structures pointed out on the frequency map are: 1) Optic Radiations, 2) Splenium of Corpus Callosum, 3) Caudate, 4) Internal Capsule, 5) Putamen, 6) Pallidum, 7) Internal Capsule.

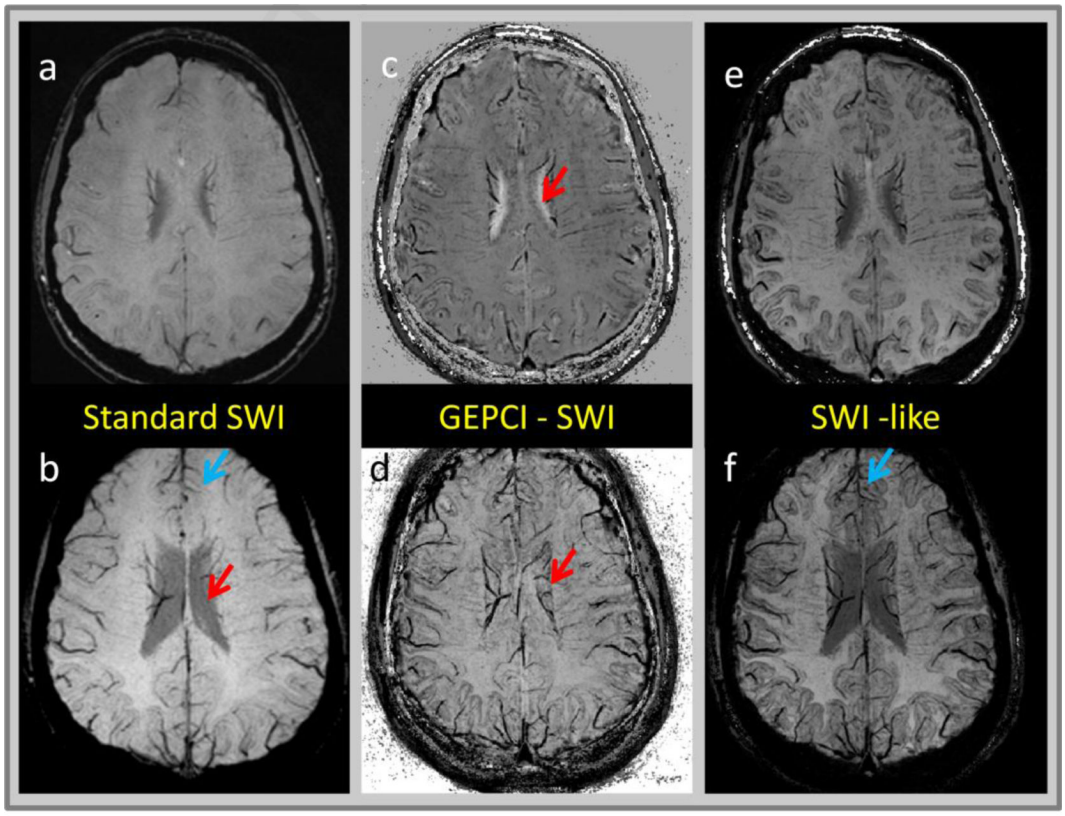

A.

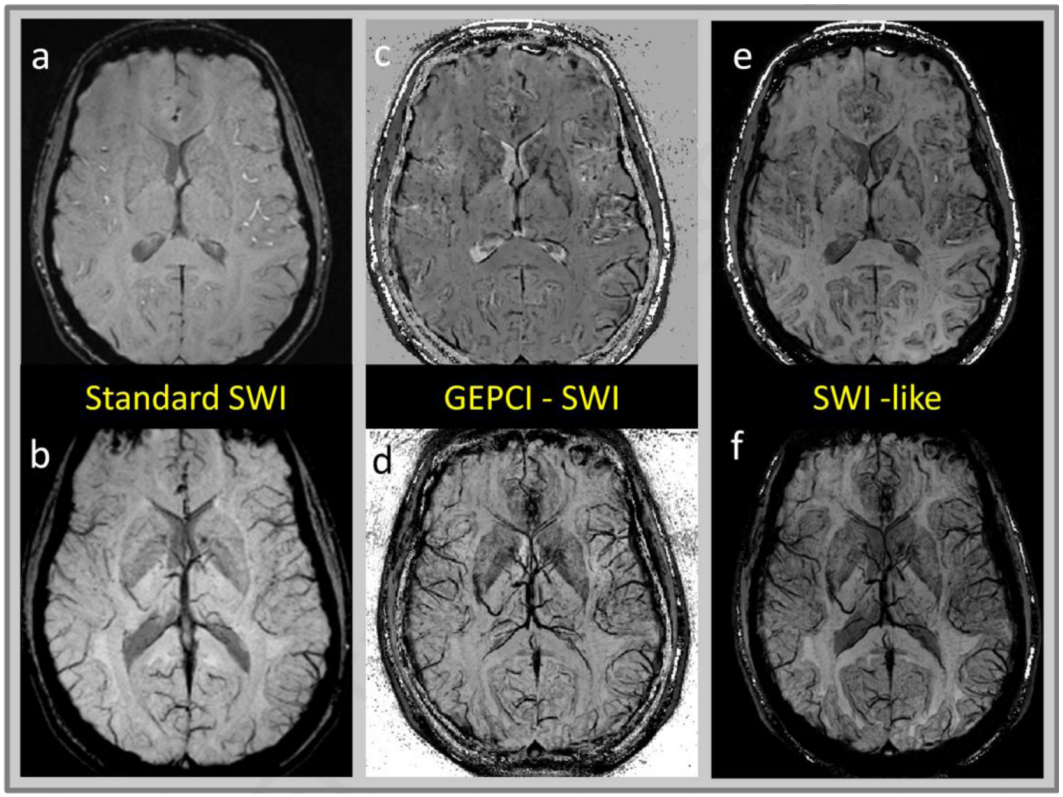

B.

Figures 4A and 4B.

Two examples of standard SWI images (left column - a,b), GEPCI-SWI images (middle column - c,d) and GEPCI-derived SWI like images (right column – e,f). The bottom row is the minIP corresponding to the images in the upper row. Standard SWI images (a & b) are obtained from Siemens automatic reconstruction. The rest of the images (c-f) are all derived from the same GEPCI 3D data set.

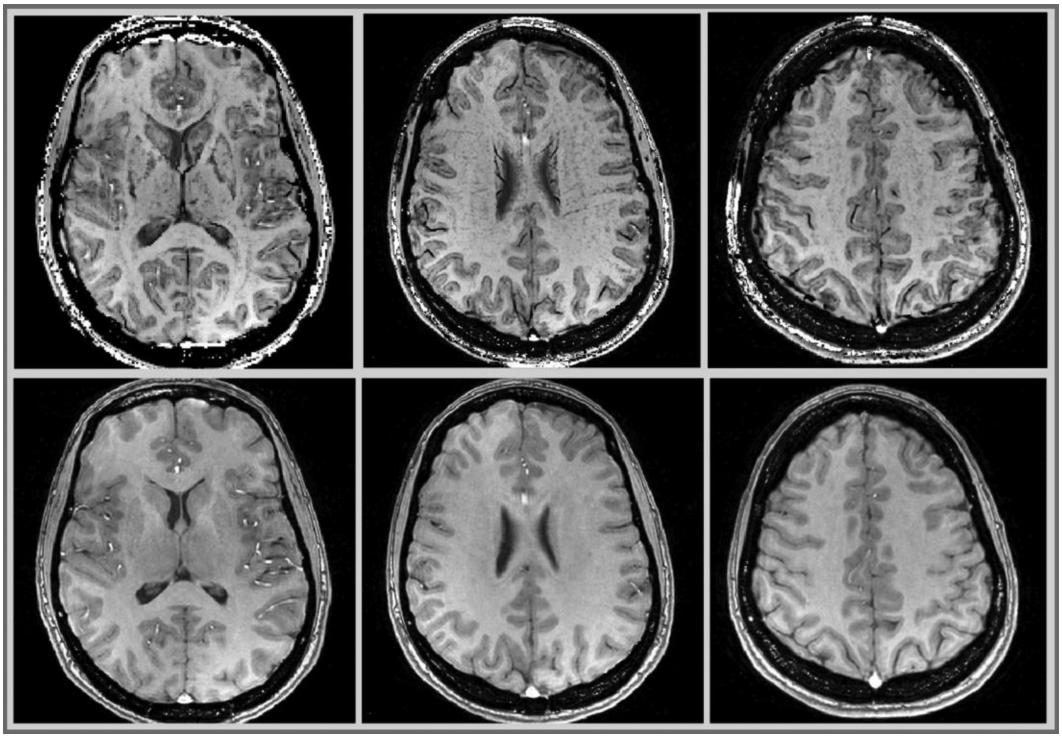

Figure 5.
Examples of the GEPCI-T1f images obtained according to Eq. (8) (top row), comparing with basic GEPCI-T1 weighted images (bottom row). GEPCI-T1f images show excellent GM/WM matter contrast. Deep grey matter structure such as caudate and putamen nuclei are also clearly outlined on the GEPCI-T1f images.

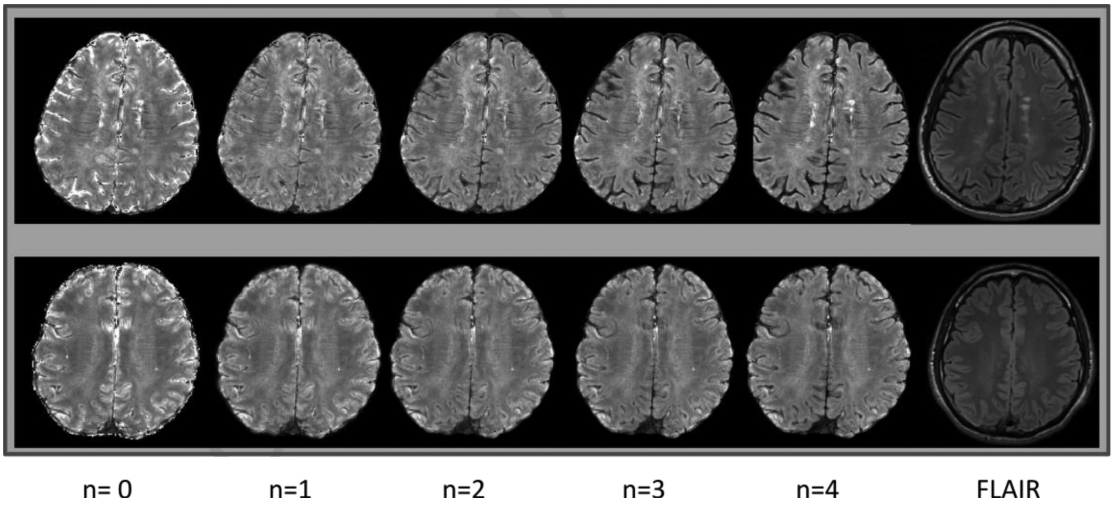

Figure 6.

Example of the FST2* images (obtained using Eq. (9) with different parameter *n*), and corresponding FLAIR T2 images. Top row – images from a subject with relapsing remitting MS, bottom row - images from a healthy subject. Different degree of suppression is shown from first column through fifth column, as parameter n grows from 0 to 4 in Eq. (9). The case with n=4 for the MS patient shows image resulted from applying suppression of n=4 with exclusion of white matter area.

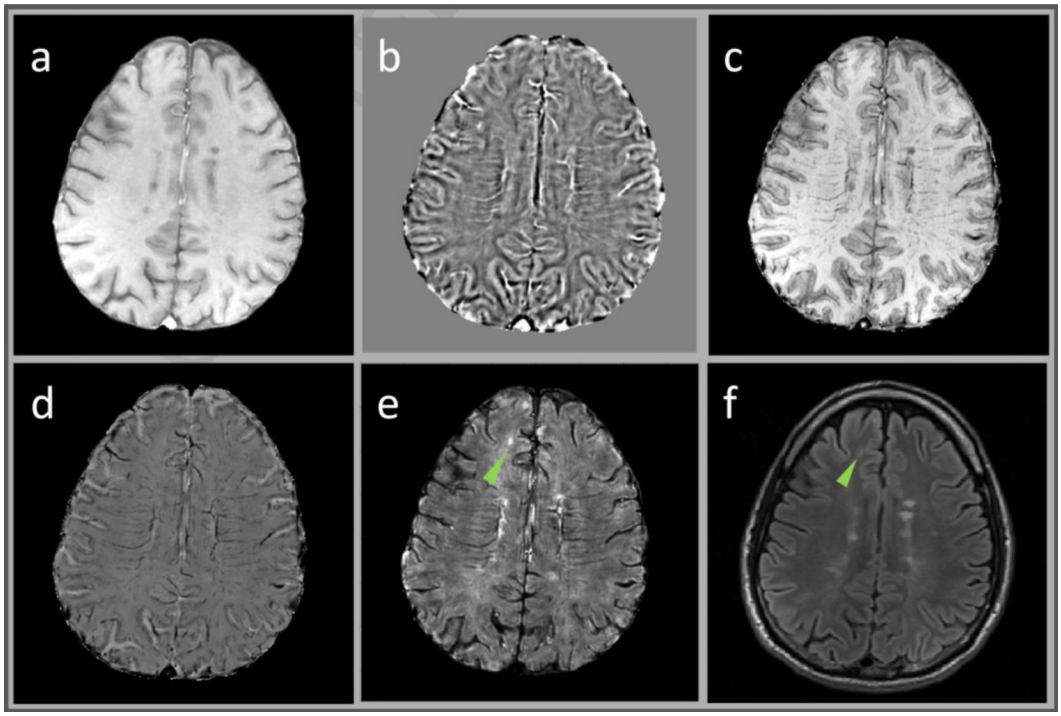

Figure 7.
Examples of a series of GEPCI images applied to disease of Multiple Sclerosis. a) GEPCI-T1weighted image; b) frequency map; c) GEPCI-T1f image; d) GEPCI-SWI image; e) T2*-SWI, result from d multiplied by FST2* image; f) FLAIR image. Most MS lesions (hyperintence on e and f) are seen around veins; green arrow indicates example of lesion that is not affiliated with identifiable blood vessels.